International Journal of Materials Engineering 2015, 5(1): 10-16
DOI: 10.5923/j.ijme.20150501.03

Growth and Corrosion Behaviour of Amorphous Micrometre Scale Calcium Phosphate Coatings on Magnesium Substrates

Derek Fawcett, Sridevi Brundavanam, Gérrard Eddy Jai Poinern*

Murdoch Applied Nanotechnology Research Group, Department of Physics, Energy Studies and Nanotechnology, School of Engineering and Energy, Murdoch University, Murdoch, Western Australia, Australia

Abstract Amorphous calcium phosphate (ACP) coatings were formed on magnesium substrates via a straightforward electrochemical technique in order to improve the corrosion resistance of the substrates. X-ray diffraction spectroscopy and microscopy techniques were used to investigate the size, morphology, composition and structure of the ACP coatings. Analysis of the ACP coatings revealed the presence of micrometre scale fissures and tubular structures. Despite the presence of these features, the coatings were still capable of significantly reducing the corrosion rate in both PBS and Ringer's solutions. Ringer's solution was found to be the most aggressive towards Mg substrates with a corrosion rate of 3.828 mm/yr. However, after electrochemical treatment, the corrosion rate of substrates coated with ACP was reduced to 0.557 mm/yr. The significant improvement in corrosion resistance is a first step in controlling the corrosion rate of biodegradable Mg substrates for potential use in hard tissue applications.

Keywords Biodegradability, Electrochemical synthesis, Magnesium, Calcium phosphates

1. Introduction

Magnesium (Mg) is a silvery coloured metal that is currently being investigated as a potential biologically degradable implant material for bone tissue engineering. Mg is a lightweight metal with a high strength to weight ratio that also has a number of advantageous properties such as good biocompatibility and biodegradable in the aqueous physiological environment of the body [1]. In terms of mechanical properties, Mg is similar in nature to bone in terms of density and elastic modulus. The density of Mg is around 1.74 g/cm^3 at 20 ℃, while bone tissue ranges from 1.8 to 2.1 g/cm^3. In terms of elastic modulus, bone tissue varies from 40 to 57 GPa and pure Mg around 45 GPa [2, 3]. Interestingly, it is the close similarity between the elastic modules that makes Mg a potential biocompatible material suitable for reducing stress shielding and preventing bone resorption. Stress shielding and the resulting bone resorption are significant problems that can be encountered with conventional metallic implant materials [4]. In addition, unlike Mg, which has been shown to be physiologically beneficial in the body [5, 6], traditional metallic implants can release toxic metallic ions such as chromium, cobalt and nickel. The release of these toxic ions during biological corrosion and mechanical wear often leads to an unfavourable immune response that significantly reduces the biocompatibility of the implant and often leads to secondary revision surgery [7, 8].

However, before Mg can be used in the manufacture of biodegradable orthopaedic implants two fundamental problems need to be addressed and both stem from the metal's rapid corrosion in chloride rich aqueous body fluids [9]. The first involves the rapid formation of hydrogen gas, which overwhelms surrounding tissues and results in the formation of subcutaneous bubbles [10, 11]. The second problem results from the rapid loss of mechanical strength and structural support between the Mg implant and the surrounding bone tissue that impedes the healing process. Therefore, effectively reducing the corrosion rate would significantly improve the mechanical and structural integrity of the implant for longer periods of time and also reduce the levels of subcutaneous gas formation. One interesting method of improving the corrosion resistance of a susceptible implant material is to coat it with a non-corrosive protective layer that is both biocompatible and bioactive. Bioactive coatings based on calcium phosphates have been successfully applied to coat variety of conventional metal implants in order to improve their biocompatibility and reduce the release of corrosion products into the human body [12].

In this study an amorphous calcium phosphate (ACP)

* Corresponding author:
G.Poinern@murdoch.edu.au (Gérrard Eddy Jai Poinern)
Published online at http://journal.sapub.org/ijme

$[Ca_9 (PO_4)_6]$ coatings were formed on magnesium substrates during a straightforward electrochemical synthesis process. The electrochemical cell consisted of two electrodes. The first electrode was a platinum wire mesh (anode) and the second was an Mg substrate that acted as the cathode. Both electrodes were immersed in an electrolyte consisting of calcium nitrate and potassium di-hydrogen phosphate. ACP has a non-crystalline character that lacks long-range periodic uniformity normally associated with crystalline structures and readily precipitates from highly saturated aqueous solutions containing calcium and phosphate ions due to its lower surface energy [13, 14]. It has a spherical structural unit composed of randomly assembled clusters of ions approximately 9.5Å in diameter and also contained within the interstices is tightly bound water, which can be as much as 20% by weight of the particle [15]. It is the metastable properties of ACP in body fluids that makes it more osteoconductive than hydroxyapatite and also gives it superior biodegradability when compared to tri-calcium phosphate [16-18]. And because of its metastable properties, ACP will transform to a more thermodynamically stable crystalline calcium phosphate phase such as hydroxyapatite via a process of dissolution, nucleation, and crystal growth [19]. Advanced characterisation techniques such as X-ray diffraction (XRD) spectroscopy, Transmission electron microscopy (TEM), Scanning electron microscopy (SEM) and Energy Dispersive Spectroscopy (EDS) were used to determine size, morphology, crystalline structure and composition of the ACP coatings formed by the electrochemical process. The corrosion resistance of the coatings was then evaluated in phosphate buffer saline (PBS) solution and Ringer's solution at body temperature (37ºC).

2. Materials and Methods

2.1. Materials

All aqueous solutions were made using Milli-Q® water (18.3 MΩ cm^{-1}) produced by an ultrapure water system (Barnstead Ultrapure Water System D11931; Thermo Scientific, Dubuque, IA). All chemicals and reagents used in this study were supplied by Chem-Supply (Australia).

2.2. Surface Pre-treatment of Mg Substrates

High purity (99.9%) Mg foil 0.15 mm in thickness was cut into rectangular strips 40 mm in length and 3 mm in width. Silicon carbide (Si C) paper (1200 grit) was used to remove all surface oxides and contaminants. After initial surface cleaning, the strips were chemically cleaned in 5% wt. nitric acid (HNO_3) solution followed by ultrasonically rinsing in acetone for 10 min. This was followed by rinsing with Milli-Q® water to remove acetone and then allowing the substrates to air dry. After drying the weight of each substrate was recorded using an Ohaus PA214C microbalance.

2.3. Electrochemical Synthesis of ACP Coatings

The electrochemical cell was composed of two electrodes and an electrolyte. The electrolyte consisted of an aqueous solution containing 0.32 M of $Ca(NO_3)_2.4H_2O$ and 0.19 M of KH_2PO_4. The electrodes consisted of a platinum wire mesh (anode) and an Mg substrate, which was used as the cathode. A standard laboratory DC power supply [GW INSTEK GPS-2303] was used to supply the required voltage range with a maximum current density of $60mA/cm^2$ in the dynamic mode setting with a fixed voltage (6 V) and variable immersion times ranging from 30 s to 5 min.

2.4. Advanced Characterisation of Coatings

2.4.1. X-ray Diffraction (XRD) Spectroscopy

XRD spectroscopy was used to identify the presence of any crystalline phases present in the surface coating formed during electrochemical synthesis. Spectroscopy data was recorded at room temperature, using a GBC® eMMA X-ray Powder Diffractometer [Cu Kα = 1.5406 Å radiation source] operating at 35 kV and 28 mA. The diffraction patterns were collected over a 2θ range of 20° to 60° with an incremental step size of 0.02 ° using flat plane geometry with 2 second acquisition time for each scan.

2.4.2. Transmission Electron Microscopy (TEM)

The size and morphology of ACP particles formed during the synthesis process were investigated using TEM. Sample material taken from substrates was placed into small tubes containing Milli-Q® water, sealed and placed into an ultrasonic bath for 10 minutes. Suspensions were then filtered 2 times before a single drop from each sample was placed onto a carbon-coated copper TEM grid using a micropipette. After a 24-hour period drying period, samples were investigated using a Phillips CM-100 electron microscope (Phillips Corporation Eindhoven, The Netherlands) operating at 80kV.

2.4.3. Scanning Electron Microscopy (SEM) and Energy Dispersive Spectroscopy (EDS)

The size and morphology of coating features formed on Mg substrates were examined using SEM, while the elemental composition of the coatings was investigated using EDS. All micrographs were taken using a JCM-6000, NeoScopeTM with attached energy dispersive X-ray spectroscopy. Samples were mounted on individual substrate holders using carbon adhesive tape before being sputter coated with a 2 nm layer of gold to prevent charge build up using a Cressington 208HR High Resolution Sputter coater.

2.5. Corrosion Resistance of ACP Coating

The corrosion resistance of pure Mg substrates and ACP coating substrates was investigated using freshly prepared

phosphate buffer saline (PBS) solution and Ringer's solution. The composition of the PBS solution (in g/L) consisted of 8.006 NaCl, 0.201 KCl, 1.420 Na_2HPO_4 and 0.240 KH_2PO_4. The Ringer's solution composition (in g/L) consisted of 8.6 NaCl, 0.6 KCl and 0.66 $CaCl_2.2H_2O$. The pH and temperature of both test solutions was maintained at 7.4 and 37 ℃ respectively so that body fluid pH and temperature could be replicated. An EG&G Princeton Potentiostat/galvanostat (Model 273A supplied EG&G Princeton applied research) using a three-electrode arrangement was used to generate polarization curves. The working electrode was a test substrate with a surface area of 1 cm^2. The remaining two electrodes consisted of a saturated calomel electrode (SCE) that was used as the reference electrode, while the counter electrode was a platinum wire (Pt.). A Tafel test procedure was performed using a voltage range between -2.5 V and 1.0 V, with a step size of 10 mV and a 1s time interval for the 10 mV scan rate. From the resulting experimental polarization curves the corrosion rate (mm/yr.) was calculated.

3. Results and Discussions

3.1. XRD Spectroscopy and TEM Analysis

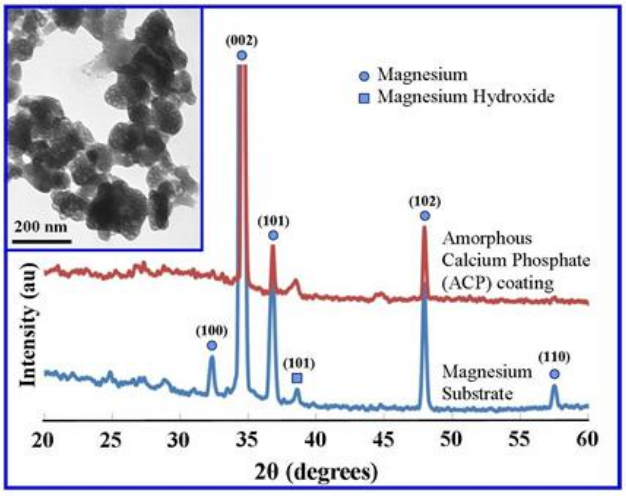

Figure 1. XRD analysis of a representative Mg substrate and ACP coated substrate, with insert TEM image of synthesized ACP particles

The XRD technique was used to examine Mg substrates before and after the electrochemical process. Figure 1 presents a representative set of XRD patterns for untreated and treated substrates. Examination of the pattern for the untreated substrate reveals the presence of six peaks over the 2θ range from 20º to 60º. The pattern contains three major peaks [(002), (101) and (102)] and two minor peaks [(100) and (110)] that correlate to the crystalline structure of the Mg substrate. Also present in the pattern was a minor peak (101) that indicated the presence of $Mg(OH)_2$ on the substrate surface. No other surface contaminants were found on the substrate. Subsequent electrochemical processing of substrates produced a thin white calcium phosphate coating over the surface. The coating was identified as amorphous calcium phosphate due to the presence of a very large broad and diffuse peak centred on the 2θ angle of 25°, characteristic of non-crystalline calcium phosphate materials [20]. However, three peaks could be seen in the XRD pattern [(002), (101) and (102)] and were identified as the underlining Mg substrate.

The inserted TEM image presented in Figure 1 is a representative of the spherical morphology and highly agglomerated nature of the ACP particles that make up the surface coatings of the treated substrates. Particle size analysis revealed that the particles ranged in size from 60 nm up to 250 nm, with a mean particle size of 120 nm.

3.2. SEM and EDS Analysis of Coating Growth

The SEM technique was used to study the growth of the ACP coating thickness during the electrochemical process. The technique was also used to investigate the surface features and structure of the coatings. Figures 2 (b), (c) and (d) present micrographs showing the growth and increasing coating thickness with treatment time. Figure 2 (a) graphically presents the growth in coating thickness and reveals that the growth rate varies during the treatment. At the end of the 5 minute treatment period, a typical coating reached on average a thickness of around 70 µm. Analysis of SEM micrographs of the coatings reveals there granular structure which can be seen throughout the cross-sections. In addition, with treatment time the coating tends to detach from the underlining substrate. Also noticeable were the very rough surfaces of the respective coatings that are exposed to the electrolyte and the presence of tubular surface features.

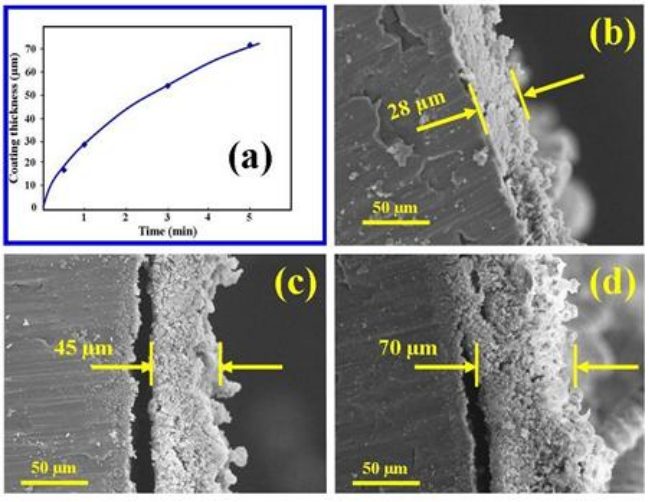

Figure 2. (a) Growth of ACP coating layer; SEM micrographs of mean thickness measurements taken during growth of coating thickness with time at 6 V potential (b) 1 min; (c) 3 min, and (d) 70 min

Further SEM investigation of the coating surface revealed a landscape covered by tubular structures and large fissures. Figure 3 (a) presents a representative landscape

showing numerous micrometre scale tubular structures formed during the electrochemical treatment. Also seen in Figure 3 (a) are the surface fissures which can be as large as 30 μm in width and zigzag across the surface for many 100's of μm's. Many of these fissures, like the tubular structures provide the electrolyte access to the underling Mg substrate. Both the fissures and tubular structures have been formed as a result of hydrogen gas evolution occurring at the metal-coating interface. Figure 3 (b) presents an enlarged view of a representative tubular formation seen in the coating. The central channel diameter of the tube was estimated to be around 45 μm and extended down through the coating to the underlining Mg substrate.

Figure 3 (c) presents the results of the EDS analysis and gives a breakdown of the elemental components present in the ACP coating. The analysis reveals the presence of significant amounts of Ca, P and K and traces of O and Mg. The mean calcium to phosphate ionic ratio (Ca:P) of the coatings was estimated to be 2.1, which is within the 1.2 to 2.2 range specified by Dorozhkin [13] for ACP. Initially, the production of ACP was fairly rapid, however, after 3 minutes the deposition rate significantly reduced as seen in Figure 3 (d). The build-up of ACP after 3 minutes, which equated to 7.6 mg in mass and a thickness of 55 μm was significantly reducing the amount of electrolyte in contact with the underlining substrate and was providing some degree of isolation from the electrolyte. And by the end of the 5 minute treatment period the mass of a representative coating was around 10 mg with a typical thickness of 70 μm. During the 3 to 5 minute treatment period the coating formation rate was around 45% lower than the 0 to 3 minute period. The EDS analysis also found the presence of small amounts of Mg in the coatings that indicate the possibility of Mg^{2+} ions being substituted for Ca^{2+} ions during the formation of the coatings. The small amounts of Mg seen in the EDS analysis may have contributed to, but was not fully responsible for the intense Mg peaks seen in the XRD. These strong Mg peaks were primarily the result of the underlining Mg substrate.

3.3. Corrosion Resistance

The corrosion behaviour of pure Mg substrates and ACP coated Mg substrates were studied by immersing substrates into two types of aqueous mediums and then generate polarization curves using a three-electrode based a Potentiostat/galvanostat device. Both the PBS solution and the Ringers solution were maintained at 37 ℃ and a pH of 7.4 during the test procedure. Representative polarization curves produced during the corrosion tests for pure Mg substrates and ACP coated substrates are presented in Figure 4. Inspection of the polarization curves of both PBS and Ringer solutions reveals that both solutions are highly corrosive to uncoated substrates. For example in seawater, the corrosion rate is typically around 0.25 mm/yr. [21], the PBS solution was calculated from the Potentiostat / galvanostat device to be 1.829 mm/yr. and Ringers solution was calculated to be 3.828 mm/yr. Clearly from these measurements it is clear that uncoated Mg substrates will rapidly corrode in these fluids without protection and explains why previous attempts of using Mg as an implant have failed to deliver satisfactory clinical outcomes. Ringer's solution was found to be the most aggressive environment for Mg substrates and this was still the case for the ACP coated substrates. The ACP coating used in the corrosion studies was able to reduce the corrosion rate from 3.828 mm/yr. down to 0.557 mm/yr. A similar trend was also seen for the tests carried out in PBS solution. In this case the original corrosion rate of 1.829 mm/yr. was reduced to 0.142 mm/yr. as listed in Table 1.

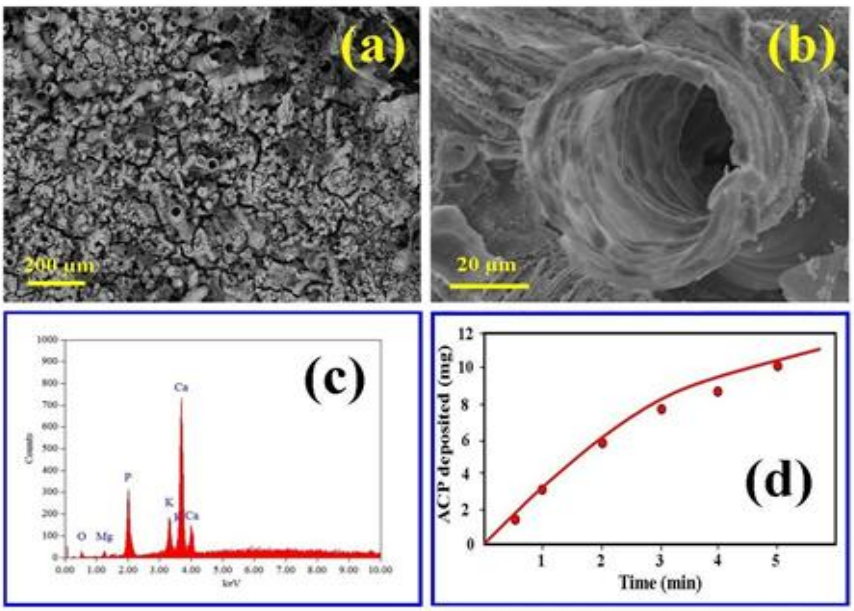

Figure 3. (a) SEM micrograph of a typical coating surface landscape; (b) enlarged view of a surface tubular structure; (c) EDS elemental analysis, and (d) deposition rate of ACP coating with time

Table 1. Corrosion rates of uncoated and ACP coated Mg substrates determined from polarization curves produced from corrosion studies carried out in PBS and Ringer's solution

Electrolyte	Sample	Corrosion Rate (mm/yr)
Humid air [21]	Mg substrate	1.0×10^{-5}
Distilled water [21]	Mg substrate	1.5×10^{-2}
Seawater [21]	Mg substrate	0.25
Phosphate buffer saline solution (This study)	Mg substrate	1.829
	ACP coated Mg substrate	0.142
Ringer's solution (This study)	Mg substrate	3.828
	ACP coated Mg substrate	0.557

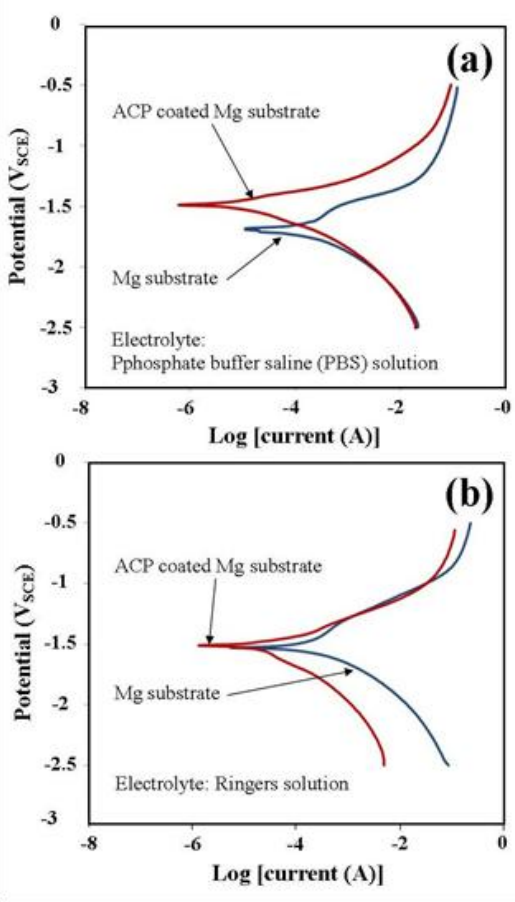

Figure 4. Polarization curves generated during corrosion testing of ACP coated Mg substrates (70 μm coating thickness) in aqueous environments at 37 ℃ and a pH of 7.4: (a) PBS solution and (b) Ringers solution

The results of the corrosion studies are interesting when you consider the structure of the ACP coating. There is clear evidence that the coating integrity is far from satisfactory, with many micrometre scale surface fissures and tubular structures present as seen in Figure 3 (a). Both of which clearly provide access to the underlining Mg substrate for the respective corrosive solutions. Also seen in SEM micrographs of coating cross-sections is clear evidence that the coating is not securely anchored to the substrate's surface. Figures 2 (c) and (d) clearly show significant detachment of the coating, with the coating lifting as much as 10 μm from the substrate surface.

The most important property of a biodegradable medical implant material is that it must slowly degrade and allow regenerating bone tissues to progressively take over from the load carrying function of the implant. In the case of Mg, the corrosion rate must be effectively controlled and thus allowing sufficient time for successful tissue regeneration to take place.

However, the rapid corrosion rates for uncoated Mg substrates recorded in this study clearly demonstrate that the mechanical integrity needed during the healing process could not be sustained for any significant length of time. Moreover, the rapid corrosion would produce the evolution of significant amounts of hydrogen gas, which surrounding tissues would find difficult to deal with. In spite of this the corrosion studies of the coated Mg substrates has shown a significant reduction in the corrosion rates for both PBS and Ringer's solutions. The studies have shown that the ACP coatings formed on the substrate surfaces during the electrochemical treatment have been able to provide some degree of protection from aggressive aqueous environments and reduce the corrosion rate. This result is important since controlling the corrosion rate of biodegradable Mg substrates is the first step in developing Mg based implants for hard tissue applications. It also provides the opportunity to develop biodegradable Mg based implants that have the potential to circumvent the long-term complications normally associated with conventional metal implants currently used in clinical applications. However, further research is needed to improve the quality and mechanical stability of the ACP coatings. I addition, further studies are needed to study the behaviour of the ACP coating in vivo since ACP is a metastable calcium phosphate phase. And as such will easily transform into more thermodynamically stable crystalline calcium phosphate phases such as hydroxyapatite via a process of dissolution, nucleation, and crystal growth [22].

4. Conclusions

A straightforward electrochemical process was used to form ACP coatings on Mg substrates with the objective of improving the corrosion resistance of the substrate. XRD spectroscopy confirmed the formation ACP on the

substrates while TEM image analysis revealed the characteristic spherical morphology normally associated with ACP particles. The image analysis also confirmed the highly agglomerative nature of the particles. SEM micrographs taken during the synthesis process reveal the formation and subsequent growth of micrometre scale tubular structures and surface fissures in the respective coatings. Despite the presence of both features, the coatings were still capable of significantly reducing the corrosion rate in both PBS and Ringer's solutions. Ringer's solution was found to be the most aggressive with a substrate corrosion rate of 3.828 mm/yr. However, the substrate corrosion rate was significantly reduced (0.557 mm/yr.) by the presence of a 70 μm ACP coating. The significant improvement in corrosion resistance of ACP coated substrates is an important result and the present study demonstrates the viability of using this electrochemical process to control the corrosion rate. Importantly, this improvement was achieved in spite of numerous tubular structures and surface fissures being produced during coating formation. The disadvantage of the ACP coating technique is unquestionably the presence of surface fissures and tubular structures. Conversely, the coatings advantages include biocompatibility, osteoconductivity, resorption potential and corrosion resistance. However, further studies are needed to build on these advantages and perhaps modifying the current electrochemical process to reduce the coating imperfections. Thus, being able to control the corrosion rate of ACP coated Mg substrates is an important first step in developing a programmable biodegradable Mg based implant for hard tissue applications.

ACKNOWLEDGEMENTS

The authors would like to thank Mr Ken Seymour for his assistance with the XRD measurements and Associate Professor Gamini Senanayake for his assistance with the electrochemical measurements. Mrs Sridevi Brundavanam would like to acknowledge Murdoch University for providing a PhD Scholarship to undertake her PhD studies.

REFERENCES

[1] Poinern, G. E.J., Brundavanam, S., Fawcett, D., 2012, Biomedical Magnesium Alloys: A Review of Material Properties, Surface Modifications and Potential as a Biodegradable Orthopaedic Implant, American Journal of Biomedical Engineering, 2(6), 218-240.

[2] Razavi, M., Fathi, M. H., Meratian, M., et al., 2010, Microstructure, mechanical properties and biocorrosion evaluation of biodegradable AZ91-FA nanocomposites for biomedical applications, Materials Science and Engineering A, 527(26), 6938-6944.

[3] Feng, A., and Han, Y., 2010, The microstructure, mechanical and corrosion properties of calcium phosphate reinforced ZK60A magnesium alloy composites, Journal of Alloys and Compounds, 504, 585-593.

[4] Ramakrishna, S., Ramalingam, M., Sampath, T. S., Soboyejo, W. O., 2010, Biomaterials: A Nano Approach, Boca Raton, USA: CRC Press, 2010, 161-186.

[5] Saris, N. L., Mervaala, E., Karppanen, H., Khawaja, J. A., Lewenstam, A., 2000, Magnesium. An update on physiological, clinical and analytical aspects, Clinica. Chimica. Acta., 294, 1-26.

[6] Kim, S. R., Lee, J. H., Kim, Y. T., et al., 2003, Synthesis of Si, Mg substituted hydroxyapatites and their sintering behaviours, Biomaterials, 24(8), 1389-1398.

[7] Lhotka, C., Szekeres, T., Steffan, I., Zhuber, K., Zweymuller, K., 2003, Four-year study of cobalt and chromium blood levels in patients managed with two different metal-on-metal total hip replacements, Journal of Orthopedic Research, 21(2), 189-195.

[8] Dearnly, P. A., 2005, A brief review of test methodologies for surface-engineered biomedical implant alloys, Surface and Coatings Technology, 198(1-3), 483-490.

[9] Mark, P. S., Alexis, M. P., Jerawala, H., Goerge, D., 2006, Magnesium and its alloys as orthopaedic biomaterials: A review, Biomaterials, 27(9), 1728-1734.

[10] McCord, C. P., 1942, Chemical gas gangrene from metallic magnesium, Industrial Medicine, 11, 71-79.

[11] Wen, C. E., Mabuchi, M., Yamada, Y., Shimojima, K. Y., Chino, Y., Asahina, T., 2001, Processing of biocompatible porous Ti and Mg. Scripta Materialia, 45(10), 1147-1153.

[12] Geetha, M., Singh, A. K., Asokamani, R., Gogia, A. K., 2009, Ti based biomaterials, the ultimate choice for orthopaedic implants – A review, Progress in Materials Science, 54, 397–425.

[13] Dorozhkin, S. V., 2009, Nano-dimensional and nano-crystalline apatite's and other calcium orthophosphates in biological engineering, biology and medicine. Materials, 2, 1975-2045.

[14] Zhao, J., Liu, Y., Sun, W. B., Zhang, H., 2011, Amorphous calcium phosphate and its application in dentistry, Chemistry Central Journal, 5(40), 1-7.

[15] Betts, F., Blumenthal, N. C., Posner, A.S., Becker, G. L., Lehninger, A. L., 1975, Atomic structure of intracellular amorphous calcium phosphate deposits. Proc. Natl. Acad. Sci., 72, 2088-2090.

[16] Li, Y. B., Li, D. X., Weng, W. J., 2007, Amorphous calcium phosphates and its biomedical application, J. Inorgan. Mater., 22, 775-782.

[17] Poinern, G. E. J., Brundavanam, R., Le, X., Nicholls, P. K., Cake, M. A., Fawcett, D., 2014, The synthesis, characterisation and in vivo study of a bioceramic for potential tissue regeneration applications, Scientific Reports, 4 (6235), 1-9.

[18] Dorozhkin, S. V., 2010, Calcium Orthophosphates as Bioceramics: State of the Art, J. Funct. Biomater., 1, 22-107.

[19] Eanes, E. D., Termine, J. D., Nylen, M. U., 1973, An

electron microscopic study of the formation of amorphous calcium phosphate and its transformation to crystalline apatite. Calcif. Tissue Res., 12, 143-158.

[20] Boskey, A. L., 1997, Amorphous Calcium Phosphate: The Contention of Bone, J. Dental. Research, 76 (8), 1433-1436.

[21] Godard, H. P., Jepson, W. P., Bothwell, M. R., Lane, R. L., Ed. The Corrosion of Light Materials, John Wiley & Sons, 1967, Chap 21.

[22] Meyer, J. L., Eanes, E. D., 1978, A thermodynamic analysis of the amorphous to crystalline calcium phosphate transformation. Calcif. Tissue Res., 25(1), 59-68.